Deficiency in gp91^{Phox} (NOX2) Protects against Oxidative Stress and Cardiac Dysfunction in Iron Overloaded Mice

I. Tong Mak [1,*], **Jay H. Kramer** [1,*], **Micaela Iantorno** [2], **Joanna J. Chmielinska** [1], **William B. Weglicki** [1] **and Christopher F. Spurney** [2]

[1] Department of Biochemistry and Molecular Medicine, The George Washington University Medical Center, Washington, DC 20037, USA; phyjch@gwu.edu (J.J.C.); wweg@gwu.edu (W.B.W.)
[2] Division of Cardiology, Children's National Medical Center, Washington, DC 20010, USA; micaela.iantorno@gmail.com (M.I.); cspurney@cnmc.org (C.F.S.)
[*] Correspondence: itmak@gwu.edu (I.T.M.); phyjhk@gwu.edu (J.H.K.)

Abstract: The role of NADPH oxidase subunit, gp91^{phox} (NOX2) in development of oxidative stress and cardiac dysfunction due to iron (Fe)-overload was assessed. Control (C57BL/6J) and gp91^{phox} knockout (KO) mice were treated for up to 8 weeks with Fe (2.5 mg/g/wk, i.p.) or Na-dextran; echocardiography, plasma 8-isoprostane (lipid peroxidation marker), cardiac Fe accumulation (Perl's staining), and CD11b+ (WBCs) infiltrates were assessed. Fe caused no adverse effects on cardiac function at 3 weeks. At 6 weeks, significant declines in left ventricular (LV) ejection fraction (14.6% lower), and fractional shortening (19.6% lower) occurred in the Fe-treated control, but not in KO. Prolonging Fe treatment (8 weeks) maintained the depressed LV systolic function with a trend towards diastolic dysfunction (15.2% lower mitral valve E/A ratio) in controls but produced no impact on the KO. Fe-treatment (8 weeks) caused comparable cardiac Fe accumulation in both strains, but a 3.3-fold elevated plasma 8-isoprostane, and heightened CD11b+ staining in controls. In KO mice, lipid peroxidation and CD11b+ infiltration were 50% and 68% lower, respectively. Thus, gp91^{phox} KO mice were significantly protected against oxidative stress, and systolic and diastolic dysfunction, supporting an important role of NOX2-mediated oxidative stress in causing cardiac dysfunction during Fe overload.

Keywords: NOX2 knockout mice; iron overload; in situ cardiac function; oxidative stress; cardiac iron; cardiac inflammation

1. Introduction

Iron overload occurs as a primary genetic disorder, or secondary to other disorders that involve excessive release or intake of iron [1]. Iron overload is a serious complication in patients receiving multiple transfusions (anemia, coronary bypass procedures) [2]. Excess iron can accumulate in several tissues, including kidney, liver, and heart [3], and is linked to enhanced injury, in a large part, through a free radical-induced lipid peroxidation (LPO) mechanism [4–7]. Transition metals such as iron, can catalytically transform via Fenton-type and Haber–Weiss reactions, and less toxic reactive oxygen species (ROS) like superoxide anion and hydrogen peroxide, to the more pro-oxidant hydroxyl radical [6]; it can also transform the less toxic lipid hydroperoxide to the more pro-oxidant alkoxyl and peroxyl free radicals. These pro-oxidants can initiate and propagate LPO, leading to tissue and functional injury [7,8]. In earlier reports [9,10], activation or induction of the vascular (endothelium) and/or inflammatory cell (neutrophils, macrophages) NADPH oxidase system [9], were implicated as an apparent source of ROS production in vivo [9,10]. However, this membrane-bound enzyme

complex (or NOX2), composed of six subunits (a Rho guanosine triphosphatase + 5-"*phox*" units), and together with p22^{phox}, is also found in myocytes [11]. Other important NADPH oxidase isoforms that exist in the myocardium include NOX4, and NOX1 [11]. NOX4 is expressed in all cardiovascular cells and generates mainly H_2O_2, whereas NOX1 is expressed mainly in vascular smooth muscle cells [11]. Most NOXs generate superoxide by transferring electrons from NADPH inside the cell across membranes, and then coupling these electrons to molecular oxygen to produce superoxide [4,6]. Thus, overproduction of superoxide at a time of excessive iron (overload), may have a deleterious systemic and organ specific injurious impact. We have previously shown that treatment with select antioxidants provided significant cardiovascular functional protection to rodents exposed to chronic iron overload [12]. However, it is unclear whether the oxidative stress resulting from NADPH oxidase activity is a major contributor to the cardiac dysfunction observed during iron overload. In this study, we have used NADPH oxidase (NOX2) knockout mice (gp91^{Phox} −/−) and non-invasive echocardiography to determine the contribution of NOX2 to Fe-overload induced oxidative stress and cardiac dysfunction.

2. Materials and Methods

2.1. Animal and Iron-Treatment Models, and gp91^{phox} Knockout Strain

All animal studies were performed according to the principles in the US Department of Health and Human Services Guide for the Care and Use of Laboratory Animals, and received prior approval from the Institutional Animal Care and Use Committees (IACUCs) of both The George Washington University (GWU IACUC # A124) and the Children's National Medical Center (CNMC IACUC # 01044). We used B6.129S6-*Cybbtm1Din*/J mice deficient in the gp91^{phox} subunit of the membrane bound NADPH oxidase (Jackson Laboratory, Bar Harbor, ME, USA). This mutation is linked to the X chromosome and thus, male mice with this mutation are hemizygotes and female mice are homozygotes [13]. We used female mice 6–8 weeks of age, and the C57BL/6J (B6) strain from the same source was used as age-matched control. Mice were maintained ad libitum on a nutritionally-balanced Teklad diet (contains 42 ppm iron, Envigo-Teklad Laboratory, Madison, WI, USA) and had free access to deionized, distilled water. Mice received biweekly i.p. injections totaling 2.5 mg iron-dextran/g body wt (or Na dextran for control) for up to 8 weeks, and in situ cardiac function was monitored prior to Fe treatment (baseline) and at 3, 6, and 8 weeks of treatment. At the time of sacrifice, blood (cardiac puncture) and cardiac tissue samples were collected to assess plasma 8-isoprostane levels (lipid peroxidation marker), cardiac CD11b+ cell staining, and iron accumulation.

2.2. Non-Invasive Echocardiography

The Visual Sonics Vevo 660 ultrasound system allows two-dimensional imaging with an axial resolution down to 60 microns and lateral resolution of 150 microns. The system is equipped with the EKVTM system (ECG-based Kilohertz Visualization), and uses electrocardiogram gating to obtain reconstructed static and 2D cineloop-based images at 250 to 1000 frames/s, compared to clinical systems (only 60–120 frames/s). This enables imaging adult mouse hearts with greater resolution. A 15 MHz probe was used to image hearts. Echocardiography was performed on anesthetized mice (2% isoflurane with 100% O_2; E-Z Anesthesia Chamber with nose cone, Euthanex Co., Palmer, PA, USA), and heart rate and rectal temperature were monitored [12,14]. Mice were placed on a heated platform with paws taped to electrode pads for monitoring [14]. Sterile lubricant was applied to prevent drying eyes, and ambient temperature was heat lamp-controlled. Thorax hair was removed and mice were imaged for 30 min and placed in 100% O_2 until fully recovered. Measured parameters: aortic and pulmonary artery diameter measurements were made to help calculate stroke volumes; left ventricular (LV) wall thickness and internal diameter were measured to detect a dilated or hypertrophic cardiomyopathy. LV internal diameters, in systole and diastole, were used to calculate shortening fraction. Spectral

Doppler velocities were measured for the pulmonic and aortic outflows to calculate cardiac output and for mitral valve inflows (E and A waves) to assess ventricular diastolic function [12,14].

2.3. Plasma 8-Isoprostane Assay

Plasma samples (with 0.005% BHT added) were processed to obtained 8-isoprostane levels measured by an established enzyme immunoassay kit (Catalog No. 516351) from Cayman Chemical (MI) as described [15,16]. Briefly, duplicate 10 and 20 µL plasma samples (in 200 µL of assay volume) were used to determine free 8-isoprostane concentrations, based on the absorbance values (410 nm) of standards at known concentration.

2.4. Iron Determinations

Cardiac tissue iron accumulation was assessed in ventricular sections (5 micron thick) from Fe- or Na-treated B6 and KO mice using Perls' Prussian blue method for trivalent Fe [17]. Iron deposits (blue staining) were examined under the Olympus BX60 microscope, and images were taken with a digital camera (Evolution Colour MP; Media Cybernetics, Silver Spring, MD, USA); magnification = 20×.

2.5. Cardiac Tissue CD11b+ Staining and Analysis

Heart tissue was rapidly excised, rinsed, quickly embedded in OCT compound, and frozen at −70 °C until used [12]. Cryo-sections (5 micron thick) of ventricles from Fe- or Na-treated B6 and KO mice were stained immunohistochemically for CD11b+ cell infiltrates using goat polyclonal anti-mouse CD11b antibody (1:250, Santa Cruz Biotechnology, Paso Robles, CA, USA),and Vectastain Elite ABC immunoperoxidase system and ImmPact VIP peroxidase substrate kits (Vector Laboratories Inc., Burlingame, CA, USA). Negative controls (primary antibody omitted) were included in all experiments [18,19]. Samples were examined under an Olympus BX60 microscope and multiple digital images were taken with a digital camera (Evolution Colour MP; Media Cybernetics, Silver Spring, MD, USA); magnification =20×. ImageJ software (Image processing and analysis in Java, http://imagej.nih.gov) was used to quantify the area of brown staining for CD11b [20]. ImageJ is the NIH public domain available program for computer-assisted analysis in bright-field microscopy. Using a lower and upper value bar for the threshold (Image/Adjust/Threshold) tool, allows segmenting the image into areas of interest, such as positively brown stained tissue, and to exclude the background. Using upper and lower bars of the saturation tool sets the saturation of the color of interest. The area included within the selected threshold was then calculated through ImageJ's measure (Analyze/Measure) tool as the number of pixels. The number of pixels in the area of interest divided by the number of pixels in the entire tissue area × 100 results in percent of positively stained area for CD11b. Micrographs from 3–4 animals per group were used for quantification.

2.6. Statistical Assessments

Analysis of variance (ANOVA) was used for statistical comparison of several means, and Tukey's test for all paired mean comparisons. Values for $p < 0.05$ were considered statistically significant.

3. Results

3.1. Weight Gain

It was reported that NOX2 is not involved in food intake behavior [21]; thus, we only examined the effects of iron overload on body weight changes. Even though they were age-matched, initial average body weight of B6 mice (20.22 g ± 0.60, N = 10) was 8.9% ± 0.26 higher than initial average KO mouse body weight (18.57 g ± 0.3, N = 10). After 8 weeks, slightly higher percentage weight gains for the Fe-treated mice were noticed in both B6 (32.6 ± 0.54% vs. 36 ± 2.6%, N.S.) and KO (29.4 ± 0.5% vs. 34.0 ± 1.7% $p = 0.05$) mice; however, these proved not to be significantly different based on actual

body weights at 8 weeks, which were: B6 + Na, 26.81 g ± 0.47 vs. B6 + Fe, 27.50 g ± 2.0, and KO + Na, 24.03 g ± 0.4 vs. KO + Fe, 24.88 g ± 1.2.

3.2. Plasma 8-Isoprostane Levels

We investigated the role of the NOX2-linked NADPH oxidase enzyme system in development of oxidative stress and cardiac dysfunction during Fe-overload. At 8 weeks, the 8-isoprostane level of the sodium-treated KO mice was 25% (N.S.) lower than B6 controls (Figure 1). With iron treatment, this marker of systemic lipid peroxidation was significantly elevated, 3.3-fold, in the B6 mice. For comparison, the elevation in the iron-treated KO mice was only 2.1-fold (Figure 1). The absolute 8-isoprostane levels of the iron-treated B6 mice were about 2-fold ($p < 0.05$) higher than that of their KO counterparts (Figure 1).
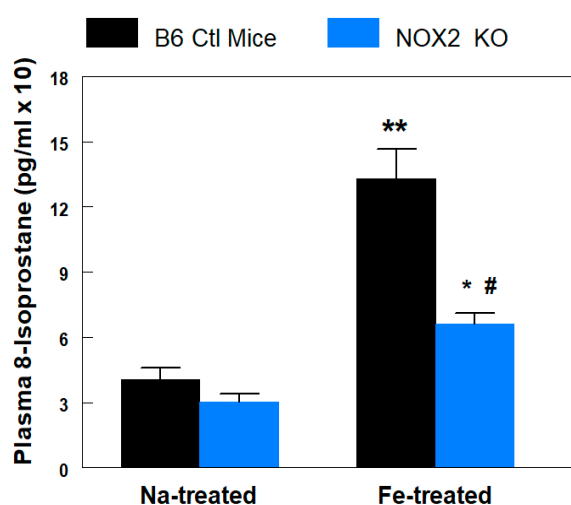
Figure 1. B6 wildtype control and NADPH oxidase 2 (NOX2) knockout (KO) mice exposed to chronic Fe-overload were compared with respect to in vivo lipid peroxidation (8-isoprostane). Plasma samples were obtained after sacrifice of B6 (8 weeks) or KO (8 weeks) mice, which received biweekly i.p. injections of Fe (2.5 mg/g/week)- or Na-dextran. Plasma 8-isoprostane levels were determined by an enzyme immunoassay kit from Cayman Chemical. Values are means ± SE of 4–5 mice. * $p < 0.05$ and ** $p < 0.01$ vs. Na-dextran treated KO and B6, respectively; # $p < 0.01$ vs. Fe-treated B6.

3.3. Cardiac Contractile Dysfunction

The cardiac contractile responses of the NOX2 KO mice were compared to B6 controls prior to iron-overload. Baseline echocardiographic parameters revealed no significant differences between B6 control and NOX2 KO mice (Table 1). After both strains of mice were treated with Fe- or Na-dextran (vehicle control), echocardiograms were performed at 3, 6, and 8 weeks. Cardiac Fe accumulation, and CD11b+ inflammatory cell infiltrates were also assessed at sacrifice (8 weeks). At 3 weeks, Fe treatment had minimal effects on echocardiographic parameters in either strain of mice (Figure 2). However at 6 weeks, significant ($p < 0.05$) decreases in left ventricular ejection fraction (A: LVEF, 14.6% lower versus time-matched Na-dextran and 19.7% lower versus time-matched Fe-treated KO), and fractional shortening (B: %FS, 19.6% lower versus time-matched Na-dextran and 26.3% lower versus time-matched Fe-treated KO) occurred in Fe-treated B6 controls, but no decreases were observed in Fe-treated KO mice. No significant changes in mitral valve E/A ratio (C: suggesting normal diastolic function) or left ventricular mass (no hypertrophy, data not shown) occurred at 6 weeks of Fe treatment in either strain. When the Fe treatment was extended to 8 weeks, LV systolic function remained depressed in B6 controls (Figure 2A,B); in addition, a significant ($p < 0.05$) diastolic dysfunction (15.2% lower versus time-matched Na-dextran) had developed (Figure 2C). Strikingly, no significant declines were found for systolic or diastolic parameters throughout 8 weeks of Fe-treatment in KO mice.

Table 1. Comparison of Baseline Echo Measurements between B6 Ctl and NOX2 KO Mice.

Echo Parameter	B6 Ctl Mice	NOX2 KO
Ao Peak Grad (mmHg)	3.40 ± 0.17	3.48 ± 0.34
Endocard. CO (mL/min)	8.14 ± 0.73	8.76 ± 0.75
LVEF (%)	70.49 ± 1.17	68.25 ± 1.21
LV FS (%)	38.63 ± 0.87	37.12 ± 0.97
LV Mass (uncorrected) (g)	70.80 ± 5.50	76.77 ± 4.80
PA Peak Grad (mmHg)	1.52 ± 0.11	1.68 ± 0.11
Heart Rate (bpm)	446 ± 24.9	421 ± 6.30
MV A (cm/s)	367.7 ± 26.0	379.6 ± 22.6
MV E at A (cm/s)	589.1 ± 24.0	623.8 ± 27.9
MV E/A	1.60 ± 0.09	1.64 ± 0.08

Values are means ± SE of 10 mice per strain, and measurements were taken prior to treatment. No significant differences in any parameter were noted between strains. Ao Peak Grad = Aortic peak pressure gradient (mmHg); Endocard. CO = endocardial cardiac output (ml/min); LVEF = left ventricular ejection fraction (%); LV FS = left ventricular fractional shortening (%); PA Peak Grad = pulmonary artery peak pressure gradient (mmHg); MV A and E, and E/A = mitral valve A and E wave velocities (cm/s) and E/A ratio.
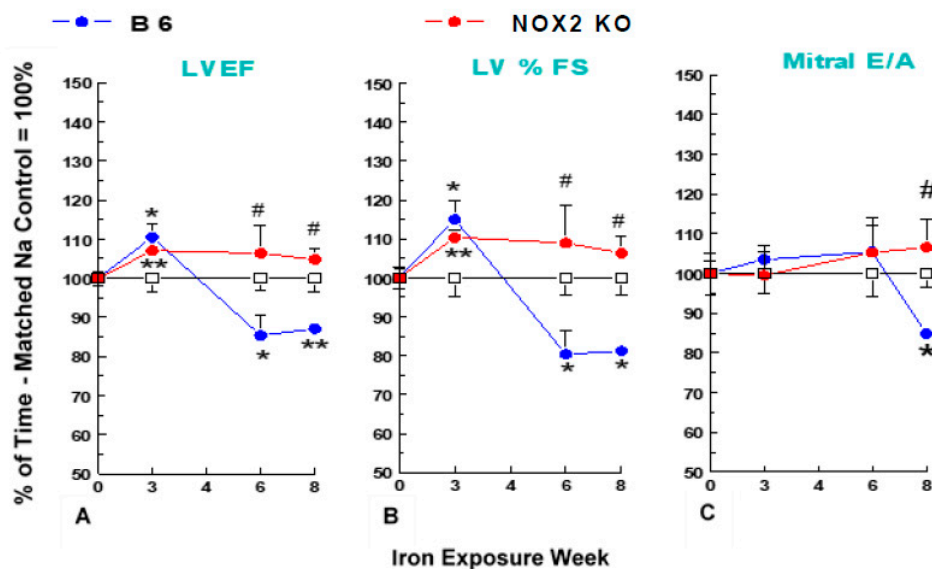

Figure 2. Iron-overload (2.5 mg/g/week Fe-dextran, i.p.) - induced cardiac dysfunction in NOX2 KO and B6 mouse strains. B6 and NOX2 KO mice received injections of Fe- or Na-dextran (Ctl) each week for up to 8 weeks, and echocardiography was performed at the described times. Percentage of time-matched Na-control values are means ± SE of 5 mice. Absent SEMs (standard error of the means) are within symbol size. No significant differences in any baseline parameter were noted between strains. (**A**) LVEF = left ventricular ejection fraction, (**B**) % FS = percentage fractional shortening; and (**C**) mitral valve E/A = mitral valve early(E)/late (atrial = A) ventricular filling velocity ratio. ** $p < 0.02$ and * $p < 0.05$ versus time-paired Na-control; # $p < 0.05$ versus time-paired Fe-treated B6.

3.4. Fe Accumulation and White Blood Cell (WBC) Infiltration

At 8 weeks, substantial cardiac Fe accumulation (Figure 3A), and heightened staining (dark brown) for cardiac CD11b+ (WBC) infiltrates in the Fe deposit areas (Figure 3B), were observed in Fe-treated B6 mice compared to its Na-treated counterpart. The enhanced cardiac Fe accumulation in KO mice (Figure 3B, left lower panels) was similar to that observed for the Fe-treated B6 group, suggesting that Fe-accumulation was not affected in this genetic model. Fe-treatment resulted in >5-fold ($p < 0.01$) elevation of CD11b+ density in B6 mice compared to the Na-dextran treated B6 controls (Figure 3C). However, CD11b+ cell staining (Figure 3B,C) was notably lower in KO mice at 8 weeks of Fe-exposure. A further quantitative estimation of the CD11b+ staining using the Image J measurement revealed

that the level of the WBC infiltration in KO mice was only about 33% ($p < 0.01$) of that displayed by the iron-treated B6 group (Figure 3C). Cardiac sections from Na-dextran treated (Fe [-]) mice of both strains exhibited comparably low staining for CD11b+ (Figure 3B,C).
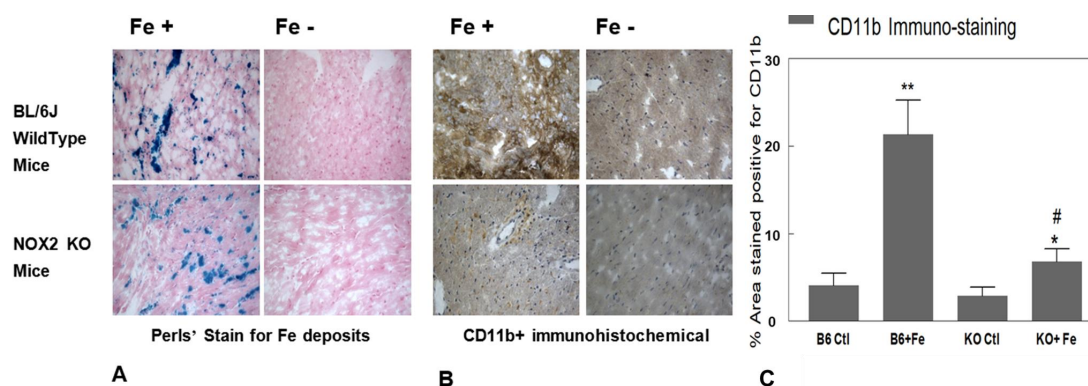
Figure 3. NADPH oxidase 2 (NOX2) knockout (KO) and B6 wildtype control mice exposed to chronic Fe-overload were compared with respect to in vivo cardiac tissue iron deposition (**A**) and cardiac CD11b+ cell infiltration (**B**). Ventricular tissue sections from B6 control (**upper panels**) and KO (**lower panels**) mice were stained for iron deposits (**A**) using Perls' method (blue) and (**B**) immunohistochemically for CD11b+ (brown). Negative controls (primary antibody omitted) were included in all immunohistochemistry experiments. Magnification 20×. (**C**) For quantification of tissue CD11b+ staining intensity ($n = 3$–5), secondary antibody conjugated to DAB (3,3′-diaminobenzidine) produced a stable brown staining of the tissue; tissues stained with DAB and observed under bright field microscope were photographed at 10 different areas per slide and were used in ImageJ analysis. * $p < 0.05$ vs. KO Ctl, ** $p < 0.01$ vs. B6 Ctl, # $p < 0.01$ vs. B6 + Fe.

4. Discussion

Higher levels of CD11b staining in the Fe-treated B6 control hearts compared to that of the KO hearts suggest elevated extent of PMN/monocyte infiltration; this would contribute at least in part to elevated oxidative stress due to the presence of the activated NADPH oxidase system in the PMNs [9,10,22]. However, it is unclear if the recruitment of PMN/monocyte infiltration occurred late and could be in response to initial myocytic oxidative injury/stimuli.

Non-phagocytic NOX2 is universally expressed in cardiomyocytes, endothelial cells, and fibroblasts [11,23]. Myocytes constitute the majority of the heart by mass [24] and could be the major contributor to contractile (dys)function. During iron-overload, circulating transferrin is saturated, and excess iron in the form of non-transferrin bound iron (NTBI) is readily taken up by major organs such as the liver, endocrine glands, and the heart [25]. NTBI may enter cardiac myocytes in the ferrous form through L-type calcium channels [26] However, excess iron accumulation in the heart was relatively delayed and in significantly lower concentration compared to that in the liver, kidney, and other tissues [1,2,27]. Yet, a high incidence of cardiomyopathy does occur in patients due to transfusional iron overload [25,27], confirming the notion that cardiomyocytes are highly susceptible to Fe-mediated injury, possibly due to the known low antioxidant activity in myocytes [28]. Iron mediated heart failure was initially manifested as systolic and/or diastolic dysfunction and arrhythmias, and by dilated cardiomyopathy in later stages [29]. As mention earlier, the catalytical properties of free iron in promoting ROS generation compounded with lower antioxidant capacity in myocyte, causes enhanced myocytic oxidative damage, which is considered an important mechanism directly contributing to iron-overload-induced cardiac dysfunction [30]. However, it remains unclear what causative role NOX2 has in the mechanism leading to iron-mediated cardiac dysfunction. In the heart, different NOX isoforms are expressed in multiple cell types including cardiomyocytes, fibroblasts, endothelial cells, and inflammatory cells [11,23]. The two main isoforms expressed in heart cells are NOX2 and NOX4 [11]. NOX2 or gp92^{phox}, together with gp62^{phox}, are plasmalemmal membrane bound, whereas

NOX4 resides in mitochondria [11]. Both isoforms require heterodimerization with a p22^{phox} subunit, but NOX2 additionally requires association with several cytosolic subunits (p47^{phox}, p67^{phox}, p40^{phox} and Rac1) to manifest full activity [11,23]. In a recent study [31], it was suggested that NOX4 mediated oxidative stress played a critical role in causing renal dysfunction in an iron overload rat model. However, its contribution to cardiac dysfunction remains unknown. In our model, it was assumed that NOX4 was still present in the KO mouse heart; yet there was no significant decreases in any contractile parameters in the Fe-treated KO mice, suggesting that NOX4 did not play a substantial role in causing Fe-mediated cardiac dysfunction. On the other hand, it was recently reported that during iron overload, NOX2 was up-regulated/activated in the vasculature of iron-overloaded animals [32]. Our current results clearly support the notion that NOX2 mediated oxidative stress plays a critical role in causing cardiac systolic and diastolic dysfunction, associated with iron overload in the mouse model. A broader role for NOX2 in contributing to heart failure was also described in a study showing that NOX2 KO protected against LV dilatation, cardiomyocyte hypertrophy, apoptosis, and interstitial fibrosis in the weeks after myocardial infarction (MI), compared to wild-type controls [33]. A separate study further indicated that myocytic rather than endothelial cell NOX2 might play a more important role in mediating post-MI remodeling [34]. Moreover, clinical findings revealed that NOX2 was upregulated in the infarcted myocardium after acute MI in patients [35].

In conclusion, gp91^{phox} KO mice were significantly protected against Fe-induced progressive oxidative/inflammatory stress and systolic/diastolic dysfunction, compared to the Fe-treated B6 controls. These findings support the concept that NADPH oxidase/NOX2 is necessary and sufficient for iron overload-mediated oxidative stress, leading to eventual development of cardiac dysfunction. Iron overload therapy has mainly been limited to removal of excess iron stores using iron-chelating agents [36]. However, all forms of chelation therapy present certain dose-limiting renal and hepatic toxicity, may suffer from compliance issues, and can be cost prohibitive [36,37]. Our findings lend support to the notion that targeting NOX2 [38] at the cardiac myocyte level could be a novel and beneficial strategy for the treatment of iron-overload induced contractile dysfunction. In recent years, a few small molecule NOX2-specific inhibitors, such GSK2795039 and VAS2870 have been developed [38,39]. GSK2795039, developed by GlaxoSmithKline, was demonstrated in vitro to be an effective and specific inhibitor of NOX2, but not of NOX1 and NOX4 [39]. Importantly, with rodent models (rat and mouse), GSK2795039 was shown to be well tolerated and bioavailable through either oral or i.p. administration. Furthermore, with a murine paw inflammation model, which is known to be induced locally by enhanced phagocytic NOX2 activity, the agent was shown to provide dose-dependent (2–100 mg/kg) attenuation of the paw inflammation associated with inhibition of tissue ROS production [39]. For comparison, other non-specific NOX inhibitors such apocynin and naloxone were not effective, whereas VAS2870 was found to be degraded rapidly in vivo. Therefore, it appears that GSK2795039 is a suitable tool molecule to further evaluate the pathophysiological role of NOX2 in Fe-mediated injury of the heart. Our future studies may employ this compound to establish dose-related protection against Fe-overload mediated cardiac dysfunction in B6 mice, and whether the effect mimics what was observed in the Fe-overload NOX2 KO model.

References

1. Zhang, H.; Zhabyeyev, P.; Wang, S.; Oudit, G.Y. Role of iron metabolism in heart failure: From iron deficiency to iron overload. *Biochim. Biophys. Acta Mol. Basis. Dis.* **2019**, *1865*, 1925–1937. [CrossRef] [PubMed]

2. Coates, T.D. Iron overload in transfusion-dependent patients. *Hematol. Am. Soc. Hematol. Educ. Program* **2019**, *2019*, 337–344. [CrossRef] [PubMed]

3. Taher, A.T.; Saliba, A.N. Iron overload in thalassemia: Different organs at different rates. *Hematology Am. Soc. Hematol. Educ. Program* **2017**, *2017*, 265–271. [CrossRef] [PubMed]

4. Imam, M.U.; Zhang, S.; Ma, J.; Wang, H.; Wang, F. Antioxidants mediate both iron homeostasis and oxidative stress. *Nutrients* **2017**, *9*, 671. [CrossRef]

5. Gunther, T.; Hollriegl, V.; Vormann, J.; Disch, G.; Classen, H.G. Effects of Fe loading on vitamin E and malondialdehyde of liver, heart and kidney from rats fed diets containing various amounts of magnesium and vitamin E. *Magnes. Bull.* **1992**, *14*, 88–93.

6. Halliwell, B.; Gutteridge, J.M.C. Oxygen free radicals and iron in relation to biology and medicine: Some problems and concepts. *Arch. Biochem. Biophys.* **1986**, *246*, 501–514. [CrossRef]

7. Berdoukas, V.; Coates, T.D.; Cabantchik, Z.I. Iron and oxidative stress in cardiomyopathy in thalassemia. *Free Radic. Biol. Med.* **2015**, *88*, 3–9. [CrossRef] [PubMed]

8. Kramer, J.H.; Misik, V.; Weglicki, W.B. Lipid peroxidation-derived free radical production and post-ischemic myocardial reperfusion injury. *Ann. N. Y. Acad. Sci.* **1994**, *723*, 180–196. [CrossRef]

9. Griendling, K.K.; Sorescu, D.; Ushio-Fukai, M. NADPH oxidase: Role in cardiovascular biology and disease. *Circ. Res.* **2000**, *86*, 494–501. [CrossRef] [PubMed]

10. Rupin, A.; Paysant, J.; Sansilverstri-Morel, P.; Lembrez, N.; Lacoste, J.M.; Cordi, A.; Verbeureu, T.J. Role of NADPH oxidase-mediated superoxide production in the regulation of E-selectin expression by Endothelial cells subjected to anoxia/reoxygenation. *Cardiovasc. Res.* **2004**, *63*, 323–330. [CrossRef]

11. Zhang, Y.; Murugesan, P.; Huang, K.; Cai, H. NADPH oxidases and oxidase crosstalk in cardiovascular diseases: Novel therapeutic targets. *Nat. Rev. Cardiol.* **2020**, *17*, 170–194. [CrossRef] [PubMed]

12. Kramer, J.H.; Spurney, C.F.; Iantorno, M.; Tziros, C.; Mak, I.T.; Weglicki, W.B. D-propranolol protects against oxidative stress and progressive cardiac dysfunction in Fe-overloaded rats. *Can. J. Physiol. Pharmacol.* **2012**, *90*, 1257–1268. [CrossRef] [PubMed]

13. Pollock, J.D.; Williams, D.A.; Gifford, M.A.; Li, L.L.; Du, X.; Fisherman, J.; Orkin, S.H.; Doerschuk, C.M.; Dinauer, M.C. Mouse model of X-linked chronic granulomatous disease, an inherited defect in phagocyte superoxide production. *Nat. Genet.* **1995**, *9*, 202–209. [CrossRef] [PubMed]

14. Spurney, C.F.; Sali, A.; Guerron, A.D.; Iantorno, M.; Yu, Q.; Gordish-Dressman, H.; Rayavarapu, S.; van der Meulen, J.; Hoffman, E.P.; Nagaraju, K. Losartan decreases cardiac muscle fibrosis and improves cardiac function in dystrophin-deficient mdx mice. *J. Cardiovasc. Pharmacol. Ther.* **2011**, *16*, 87–95. [CrossRef]

15. Zghoul, N.; Alam-Eldin, N.; Mak, I.T.; Silver, B.; Weglicki, W.B. Hypomagnesemia in diabetes patients: Comparison of serum and intracellular measurement of responses to magnesium supplementation and its role in inflammation. *Diabetes Metab. Syndr. Obes.* **2018**, *11*, 389–400. [CrossRef]

16. Mak, I.T.; Chmielinska, J.J.; Spurney, C.F.; Weglicki, W.B.; Kramer, J.H. Combination ART-induced oxidative/nitrosative stress, neurogenic inflammation and cardiac dysfunction in HIV-1 transgenic (Tg) rats: Protection by Mg. *Int. J. Mol. Sci.* **2018**, *19*, 2409. [CrossRef]

17. Luna, L.G. (Ed.) *Manual of Histologic Staining Methods of the Armed Forces Institute of Pathology*, 3rd ed.; Blakiston Division, McGraw-Hill: New York, NY, USA, 1968; pp. 184–185.

18. Mak, I.T.; Kramer, J.H.; Chen, X.; Chmielinska, J.J.; Spurney, C.F.; Weglicki, W.B. Mg-supplementation attenuates ritonavir-induced hyperlipidemia, oxidative stress and cardiac dysfunction in rats. *Am. J. Physiol. Regul. Integr. Comp. Physiol.* **2013**, *305*, R1102–R1111. [CrossRef]

19. Mak, I.T.; Chmielinska, J.J.; Kramer, J.H.; Weglicki, W.B. AZT-induced oxidative cardiovascular toxicity: Attenuation by Mg-supplementation. *Cardiovasc. Toxicol.* **2009**, *9*, 78–85. [CrossRef]

20. Chmielinska, J.J.; Kramer, J.H.; Mak, I.T.; Spurney, C.F.; Weglicki, W.B. Substance P receptor blocker, aprepitant, inhibited cutaneous and other neurogenic inflammation side effects of the EGFR1-TKI, erlotinib. *Mol. Cell Biochem.* **2020**, *465*, 175–185. [CrossRef]

21. Pepping, J.K.; Freeman, L.R.; Gupta, S.; Keller, J.N.; Bruce-Keller, A.J. NOX2 deficiency attenuates markers of adiposopathy and brain injury induced by high-fat diet. *Am. J. Physiol. Endocrinol. Metab.* **2013**, *304*, E392–E404. [CrossRef]

22. El-Benna, J.; Dang, P.M.; Gougerot-Pocidalo, M.A.; Marie, J.C.; Braut-Boucher, F. P47^{phox}, the phagocyte NADPH oxidase/NOX2 organizer: Structure, phosphorylation and implication in diseases. *Exp. Mol. Med.* **2009**, *41*, 217–225. [CrossRef]

23. Shah, A.M. Parsing the role of NADPH oxidase enzymes and reactive oxygen species in heart failure. *Circulation* **2015**, *131*, 602–604. [CrossRef] [PubMed]

24. Günthel, M.; Barnett, P.; Christoffels, V.M. Development, proliferation, and growth of the mammalian heart. *Mol. Ther.* **2018**, *26*, 1599–1609. [CrossRef] [PubMed]

25. Brissot, P.; Ropert, M.; Le Lan, C.; Loréal, O. Non-transferrin bound iron: A key role in iron overload and iron toxicity. *Biochim. Biophys. Acta* **2012**, *1820*, 403–410. [CrossRef] [PubMed]

26. Knutson, M.D. Non-transferrin-bound iron transporters. *Free Radic. Biol. Med.* **2019**, *133*, 101–111. [CrossRef] [PubMed]

27. Dimitrios, T.; Kremastinos, D.T.; Farmakis, D. Iron overload cardiomyopathy in clinical practice. *Circulation* **2011**, *124*, 2253–2263.

28. Di Meo, S.; Venditti, P.; De Leo, T. Tissue protection against oxidative stress. *Experientia* **1996**, *52*, 786–794. [CrossRef]

29. Aronow, W.S. Management of cardiac hemochromatosis. *Arch. Med. Sci.* **2018**, *14*, 560–568.

30. Kolnagou, A.; Michaelides, Y.; Kontos, C.; Kyriacou, K.; Kontoghiorghes, G.J. Myocyte damage and loss of myofibers is the potential mechanism of iron overload toxicity in congestive cardiac failure in thalassemia. Complete reversal of the cardiomyopathy and normalization of iron load by deferiprone. *Hemoglobin* **2008**, *32*, 17–28. [CrossRef]

31. Cavdar, Z.; Oktan, M.A.; Ural, C.; Calisir, M.; Kocak, A.; Heybeli, C.; Yildiz, S.; Arici, A.; Ellidokuz, H.; Celik, A.; et al. Renoprotective effects of alpha lipoic acid on iron overload-induced kidney injury in rats by suppressing NADPH oxidase 4 and p38 MAPK signaling. *Biol. Trace Elem. Res.* **2020**, *193*, 483–493. [CrossRef]

32. Ribeiro Júnior, R.F.; Marques, V.B.; Nunes, D.O.; Stefanon, I.; Dos Santos, L. Chronic iron overload induces functional and structural vascular changes in small resistance arteries via NADPH oxidase-dependent O_2^- production. *Toxicol. Lett.* **2017**, *279*, 43–52. [CrossRef] [PubMed]

33. Looi, Y.H.; Grieve, D.J.; Siva, A.; Walker, S.J.; Anilkumar, N.; Cave, A.C. Involvement of Nox2 NADPH oxidase in adverse cardiac remodeling after myocardial infarction. *Hypertension* **2008**, *51*, 319–325. [CrossRef] [PubMed]

34. Sirker, A.; Murdoch, C.E.; Protti, A.; Sawyer, G.J.; Santos, C.X.; Martin, D.; Zhang, X.; Brewer, A.C.; Zhang, M.; Shah, A.M. Cell-specific effects of Nox2 on the acute and chronic response to myocardial infarction. *J. Mol. Cell. Cardiol.* **2016**, *98*, 11–17. [CrossRef]

35. Krijnen, P.A.J.; Meischl, C.; Hack, C.E.; Meijer, C.J.L.M.; Visser, C.A.; Roos, D. Increased Nox2 expression in human cardiomyocytes after acute myocardial infarction. *J. Clin. Pathol.* **2003**, *56*, 194–199. [CrossRef] [PubMed]

36. Shah, N.R. Advances in iron chelation therapy: Transitioning to a new oral formulation. *Drugs Context* **2017**, *6*, 212502. [CrossRef]

37. Mobarra, N.; Shanaki, M.; Ehteram, H.; Nasiri, H.; Sahmani, M.; Saeidi, M.; Goudarzi, M.; Pourkarim, H.; Azad, M. A review on iron chelators in treatment of iron overload syndromes. *Int. J. Hematol. Oncol. Stem Cell Res.* **2016**, *10*, 239–247.

38. Altenhöfer, S.; Radermacher, K.A.; Kleikers, P.W.; Wingler, K.; Schmidt, H.H. Evolution of NADPH oxidase inhibitors: Selectivity and mechanisms for target engagement. *Antioxid. Redox Signal.* **2015**, *23*, 406–427.

39. Hirano, K.; Chen, W.S.; Chueng, A.L.; Dunne, A.A.; Seredinina, T.; Filippova, A.; Ramachandran, S.; Brideges, A.; Chaudry, L.; Pettman, G.; et al. Discovery of GSK2795039, a novel small molecule NADPH oxidase 2 inhibitor. *Antioxid. Redox Signal.* **2015**, *23*, 358–374. [CrossRef]